Inorg. Chem. **2005**, *44*, 979–988

Formation of CH_3TiX, $CH_2{=}TiHX$, and $(CH_3)_2TiX_2$ by Reaction of Methyl Chloride and Bromide with Laser-Ablated Titanium Atoms: Photoreversible α-Hydrogen Migration

Han-Gook Cho† and Lester Andrews*

Department of Chemistry, University of Virginia, P.O. Box 400319, Charlottesville, Virginia 22904-4319

Received October 5, 2004

The simple methylidene ($CH_2{=}TiHX$) and Grignard-type (CH_3TiX) complexes are produced by reaction of methyl chloride and bromide with laser-ablated Ti atoms and isolated in a solid Ar matrix, and they form a persistent photoreversible system via α-hydrogen migration between the carbon and titanium atoms. The Grignard-type product is transformed to the methylidene complex upon UV (240 nm < λ < 380 nm) irradiation and vice versa with visible (λ > 530 nm) irradiation. More stable dimethyl dihalide complexes [$(CH_3)_2TiX_2$] are also identified, whose relative concentration increases upon annealing and at high methyl halide concentration. The reaction products are identified with three different groups of absorptions on the basis of the behaviors upon broadband photolysis and annealing, and the vibrational characteristics are in a good agreement with DFT computation results.

Introduction

High-oxidation-state alkylidene ($M{=}CR_1R_2$) and alkylidyne ($M{\equiv}CR$) complexes have been the subject of numerous studies since the first discovery of the high-oxidation-state transition-metal complexes containing a multiple metal−carbon bond in 1970s.[1] Not only have these investigations provided a wealth of information on the nature of metal coordination chemistry, but these compounds are industrially important as metathesis catalysts for alkenes, alkynes, and cyclic compounds.[1−4] The transition-metal methylidene derived from a simple halomethane has been the subject of various theoretical studies for molecular structure and reactivity.[5−7]

The very simple $CH_2{=}M$ species have been prepared in an elegant series of late transition metal Cr through Zn reactions with diazomethane in excess argon.[8] These molecules exhibit C=M stretching frequencies in the range from 513.7 (Zn) to 696.2 (Ni) cm^{-1}.

Recently, early-transition-metal methylidenes have been observed in reactions of laser-ablated transition-metal atoms and methyl fluorides in excess argon during condensation.[9−12] More recently, a methylidene complex was formed in the reaction of methane and laser-ablated atomic zirconium.[13,14] Interestingly enough, the agostic interaction[15−17] involving the carbon and metal atoms and one of the α-hydrogen atoms is observed in these simple methylidene hydride complexes experimentally[13,14] as well as theoretically.[9−14] Moreover, persistent photoreversibility has been observed from the systems containing $CH_2{=}ZrH_2$,[14] $CH_2{=}ZrHF$,[11] and $CH_2{=}TiHF$.[9]

In the zirconium systems, the photoreversibility is believed to involve the zirconium center and two different argon

* To whom correspondence should be addressed. E-mail: lsa@virginia.edu.
† Current address: Department of Chemistry, University of Incheon, 177 Dohwa-dong Nam-ku, Incheon, 402-749 South Korea.

(1) Schrock, R. R. *Chem. Rev.* **2002**, *102*, 145.
(2) Buchmeiser, M. R. *Chem. Rev.* **2000**, *100*, 1565.
(3) Legzdins, P.; Tran, E. *J. Am. Chem. Soc.* **1997**, *119*, 5071.
(4) Choi, S.-H.; Lin, Z. *Organometallics* **1999**, *18*, 5488.
(5) Franci, M. M.; Pietro, W. J.; Hout, R. F., Jr.; Hehre, W. J. *Organometallics* **1983**, *2*, 281; *Organometallics* **1983**, *2*, 815.
(6) Cundari, T. R.; Gordon, M. S. *J. Am. Chem. Soc.* **1992**, *114*, 539.
(7) Siegbahn, P. E. M.; Blomberg, M. R. A. *Organometallics* **1994**, *13*, 354.
(8) Billups, W. E.; Chang, S.-C.; Margrave, J. L.; Hauge, R. H. *Organometallics* **1999**, *18*, 3551 and references therein to previous work in the late transition metal series.
(9) Cho, H.-G.; Andrews, L. *J. Phys. Chem. A* **2004**, *108*, 6294.
(10) Cho, H.-G.; Andrews, L. *Inorg. Chem.* **2004**, *43*, 5253.
(11) Cho, H.-G.; Andrews, L. *J. Am. Chem. Soc.* **2004**, *126*, 10485.
(12) Cho, H.-G.; Andrews, L. *Organometallics* **2004**, *23*, 4357.
(13) Andrews, L.; Cho, H.-G.; Wang, X. *Angew. Chem.* **2005**, *117*, 115.
(14) Cho, H.-G.; Wang, X.; Andrews, L. *J. Am. Chem. Soc.* **2005**, *127*, 465.
(15) Wada, K.; Craig; B. Pamplin, C. B.; Legzdins, P.; Patrick, B. O.; Tsyba, I.; Bau, R. *J. Am. Chem. Soc.* **2003**, *125*, 7035.
(16) Ujaque, G.; Cooper, A. C.; Maseras, F.; Eisenstein, O.; Caulton, K. G. *J. Am. Chem. Soc.* **1998**, *120*, 361.
(17) Scherer, W.; McGrady, G. S. *Angew. Chem., Int. Ed.* **2004**, *43*, 1782.

10.1021/ic048615a CCC: $30.25
Published on Web 01/15/2005

matrix configurations.[11] The conversion is most likely initiated by transition between the singlet and triplet CH_2═ZrH_2 or CH_2═ZrHF states, giving two different matrix cage structures. On the other hand, the photoreversibility between CH_2═TiHF and CH_3TiF occurs via α-hydrogen migration.[9] The concentration of CH_2═TiHF is relatively low initially after co-deposition of the laser-ablated metal atoms and methyl fluoride, but the concentration increases significantly upon UV irradiation of CH_3TiF. The dimethyl dihalide complex [$(CH_3)_2TiF_2$] has also been identified,[10] and the relative concentration increases dramatically upon annealing and at higher concentration of the methyl halide while those of the smaller complexes decrease.

It is therefore necessary to examine whether other methyl halides also form similar methylidene complexes and even photoreversible systems. Previous studies show that methyl fluoride is more reactive with vaporized metal atoms than methane.[11,14] The higher reactivity is considered to originate from the lone electron pairs on the halogen atom, which attract the electron-deficient metal atom. In this regard, methyl chloride and bromide would be even more reactive with vaporized transition metals. Previous studies also show that the molecular distortion due to the agostic interaction[15−17] between the metal and α-hydrogen atoms decreases in the order of Ti > Zr > Hf,[12] and therefore, another interesting question is how the agostic interaction varies with the halogen substituent on the metal center.

In this study, reactions of laser-ablated Ti atoms with methyl chloride and bromide diluted in argon were carried out, and the products isolated in a solid argon matrix were investigated by means of infrared spectroscopy. Results indicate that there are at least three different groups of absorptions on the basis of the behaviors upon photolysis and annealing, and interestingly enough, two of them form a persistent photoreversible system in the matrix. Another group of absorptions arises from a larger complex, the dimethyl titanium dihalide. The vibrational characteristics of the product absorptions are confirmed by isotopic substitution and agreement with DFT-calculated frequencies.

Experimental and Computational Methods

Laser-ablated titanium atoms (Johnson-Matthey) were reacted with CH_3Cl, CH_3Br, CD_3Br (Cambridge Isotope Laboratories, 99%), and CD_3Cl (synthesized from $HgCl_2$ and CD_3Br) in excess argon during condensation at 7 K using a closed-cycle He refrigerator (Air Products HC-2). The methods are described in detail elsewhere.[18] Concentrations of gas mixtures range between 0.2% and 0.5% in argon. After reaction, infrared spectra were recorded at a resolution of 0.5 cm^{-1} using a Nicolet 550 spectrometer with a HgCdTe detector. Samples were later irradiated by a combination of optical filters and a mercury arc lamp (175 W, globe removed) and annealed, and more spectra were recorded.

Complementary density functional theory (DFT) calculations were carried out using the Gaussian 98 package,[19] B3LYP density functional, and 6-311++G(2d,p) basis sets for C, H, F, and Ti to provide a consistent set of vibrational frequencies for the reaction products. Geometries were fully relaxed during optimization, and the optimized geometry was confirmed via vibrational analysis. All vibrational frequencies were calculated analytically, and the zero-point energy is included in calculation of the binding energies.

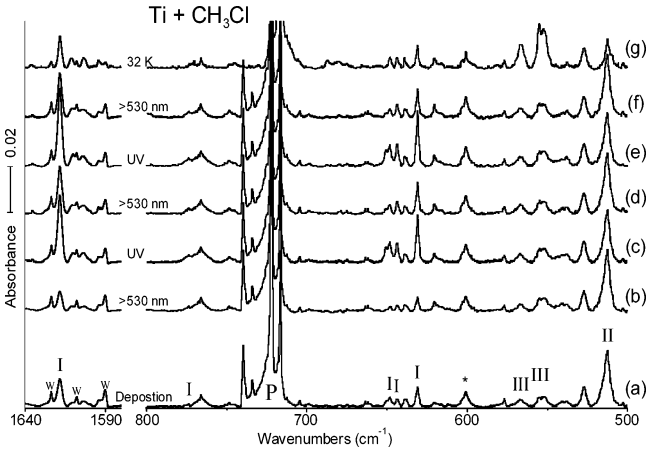

Figure 1. IR spectra in the regions of 1580−1640 and 500−800 cm^{-1} for laser-ablated Ti atoms co-deposited with CH_3Cl diluted in Ar at 7 K. (a) Ti + 0.2% CH_3Cl in Ar co-deposited for 1 h. (b) After broadband photolysis with a filter (λ > 530 nm) for 20 min. (c) After broadband photolysis with a UV-transmitting filter (240 nm < λ < 380 nm) for 20 min. (d) After broadband photolysis with a filter (λ > 530 nm) for 20 min. (e) After broadband photolysis with a UV-transmitting filter (240 nm < λ < 380 nm) for 20 min. (f) After broadband photolysis with a filter (λ > 530 nm) for 20 min. (g) After annealing to 32 K. I, II, and III stand for the product band groups, and P indicates the strong C−Cl stretching absorption of CH_3Cl. The absorptions of water impurity are marked w, and unidentified absorptions are marked with ∗.

Results and Discussion

Figure 1 shows the IR spectra in the regions of 1580−1640 and 500−800 cm^{-1} for laser-ablated Ti atoms co-deposited with 0.2% CH_3Cl in argon at 7 K and their variation upon photolysis and annealing. In the region of 1580−1640 cm^{-1}, the product absorption at 1618.4 cm^{-1} is clearly distinguished from the absorptions of water residue. Photolysis with a broadband Hg lamp and filter (λ > 530 nm), after the co-deposition, decreases the absorption. Whereas photolysis with shorter wavelength (380 < λ < 530 nm) does not produce a noticeable change in the absorption at 1618.4 cm^{-1}, UV photolysis (240 nm < λ < 380 nm) causes a dramatic increase in the intensity. The absorption later weakens in the subsequent photolysis with visible light (λ > 530 nm) but increases again in the next UV photolysis.

An analogous absorption is observed at 1619.0 cm^{-1} in the spectrum of Ti + CH_3Br (Figure 2). Initially, it is weaker

(18) (a) Chertihin, G. V.; Andrews, L. *J. Phys. Chem.* **1995**, *99*, 6356. (b) Andrews, L.; Citra, A. *Chem. Rev.* **2002**, *102*, 885 and references therein.

(19) Frisch, M. J.; Trucks, G. W.; Schlegel, H. B.; Scuseria, G. E.; Robb, M. A.; Cheeseman, J. R.; Zakrzewski, V. G.; Montgomery, J. A., Jr.; Stratmann, R. E.; Burant, J. C.; Dapprich, S.; Millam, J. M.; Daniels, A. D.; Kudin, K. N.; Strain, M. C.; Farkas, O.; Tomasi, J.; Barone, V.; Cossi, M.; Cammi, R.; Mennucci, B.; Pomelli C.,; Adamo, C.; Clifford, S.; Ochterski, J.; Petersson, G. A.; Ayala, P. Y.; Cui, Q.; Morokuma, K.; Rega, N.; Salvador, P.; DanneTierg, J. J.; Malick, D. K.; Rabuck, A. D.; Raghavachari, K.; Foresman, J. B.; Cioslowski, J.; J. V. Ortiz,; Baboul, A. G.; Stefanov, B. B.; Liu, G.; Liashenko, A.; Piskorz, P.; Komaromi, I.; Gomperts, R.; Martin, R. L.; Fox, D. J.; Keith, T.; Al-Laham, M. A.; Peng, C. Y.; Nanayakkara, A.; Challacombe, M.; Gill, P. M. W.; Johnson, B.; Chen, W.; Wong, M. W.; Andres, J. L.; Gonzalez, C.; Head-Gordon, M.; Replogle, E. S.; Pople, J. A. *Gaussian 98*, revision A.11.4; Gaussian, Inc.: Pittsburgh, PA, 2002.

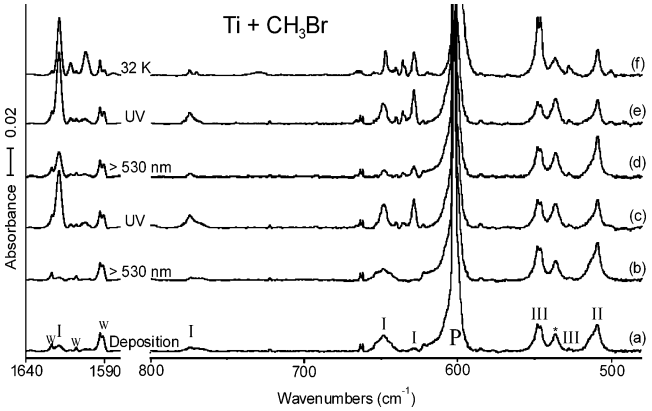

Figure 2. IR spectra in the regions of 1580−1640 and 480−800 cm^{-1} for laser-ablated Ti atoms co-deposited with Ar/CH_3Br at 7 K. (a) Ti + 0.5% CH_3Br in Ar co-deposited for 1 h. (b) After broadband photolysis with a filter (λ > 530 nm) for 20 min. (c) After broadband photolysis with a UV-transmitting filter (240 nm < λ < 380 nm) for 20 min. (d) After broadband photolysis with a filter (λ > 530 nm) for 20 min. (e) After broadband photolysis with a UV-transmitting filter (240 nm < λ < 380 nm) for 20 min. (f) After annealing to 32 K. I, II, and III stand for the product band groups, and P indicates the strong C−Br stretching absorption of CH_3Br. The absorptions of water impurity marked with w, and unidentified absorptions are marked with ∗.

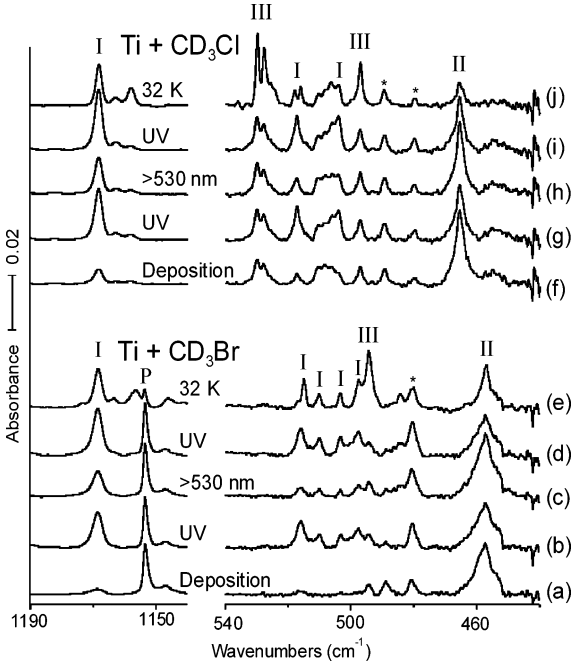

Figure 3. IR spectra in the regions of 1140−1190 and 440−540 cm^{-1} for laser-ablated Ti atoms co-deposited with CD_3Cl and CD_3Br diluted in Ar at 7 K. (a) Ti + 0.5% CD_3Br in Ar co-deposited for 1 h. (b) After broadband photolysis with a UV-transmitting filter (240 nm < λ < 380 nm) for 20 min. (c) After broadband photolysis with a filter (λ > 530 nm) for 20 min. (d) After broadband photolysis with a UV-transmitting filter (240 nm < λ < 380 nm) for 20 min. (e) After annealing to 32 K. (f) Ti + 0.5% CD_3Cl in Ar co-deposited for 1 h. (g) After broadband photolysis with a UV-transmitting filter (240 nm < λ < 380 nm) for 20 min. (h) After broadband photolysis with a filter (λ > 530 nm) for 20 min. (i) After broadband photolysis with a UV-transmitting filter (240 nm < λ < 380 nm) for 20 min. (j) After annealing to 32 K. I, II, and III indicate the product band groups. The P and ∗ labels indicate precursor and unidentified product absorptions, respectively.

after co-deposition, but it grows more significantly (more than 5-fold) upon UV photolysis. The absorptions at 1618.4 and 1619.0 cm^{-1} in Figures 1 and 2 show similar large isotopic shifts of −449.9 and −450.5 cm^{-1} upon deuteration (H/D isotopic ratios of 1.385 and 1.386) and are attributed to the Ti−H stretching mode of the reaction products of Ti + CH_3Cl and Ti + CH_3Br. Earlier studies also show that the hydrogen stretching absorptions of titanium hydrides appear in the same frequency region.[20,21] This indicates that C−H insertion by the metal atom readily occurs in the reaction of methyl halide with laser-ablated Ti atoms and even more in UV photolysis afterward.[9]

Similar alternating variations in absorption intensities on photolysis are also observed below 800 cm^{-1}, accompanied by the variations in the hydrogen stretching region, as shown in Figures 1−3. It is notable that the strong absorption at 512.5 cm^{-1} in Figure 1 decreases on UV photolysis, whereas the neighboring absorptions at 631.0, 643.8, and 648.3 cm^{-1} along with the broad absorption at 774 cm^{-1} increase dramatically (about 3-fold) similarly to the Ti−H stretching absorption in Figure 1. Subsequent photolysis with visible light (λ > 530 nm) leads to a reversal. The same variations in absorption intensities are observed repeatedly in the subsequent cycles of irradiation with UV and visible light without any noticeable decrease in the absorption intensities. Similar spectral variations are also observed in Figures 2 and 3.

Apparently, UV irradiation is more effective than visible irradiation, despite the lower intensity in the short-wavelength region. About 3 times longer visible irradiation is necessary to counteract the variation in absorption intensity caused by UV (240 nm < λ < 380 nm) irradiation. It is also notable that, whereas many product absorptions show dramatic changes in the course of photolysis, the absorptions at 552.6, 555.2, and 566.5 cm^{-1} in Figure 1 increase only gradually regardless of irradiation wavelength and later increase dramatically upon annealing. Absorptions showing similar behaviors are also observed in Figures 2 and 3.

Reactions of both methyl chloride and bromide yield similar product absorptions, and their variations upon photolysis, annealing, change in concentration, and deuteration are also comparable, as shown in Figures 1−3. Their vibrational characteristics and variations are, in turn, consistent with those in the previous study (Ti + CH_3F).[9,10] Moreover, both CH_3Cl and CH_3Br are apparently more reactive with vaporized Ti atoms than CH_3F. Under the same experimental conditiond, the product absorptions from CH_3Cl and CH_3Br are generally 2−3 times stronger than those from CH_3F.

On the basis of the above behavior, observed product absorptions are sorted into three groups as listed in Table 1, and the frequencies are compared with the calculated values in Tables 2−5. Group I absorptions are relatively weak in the original spectrum after co-depositon of methyl halide and Ti atoms, but increase dramatically (at least 3-fold) upon UV irradiation. The Ti−H and Ti−D stretching absorptions in the regions of 1580−1640 and 1140−1190 cm^{-1} shown in Figures 1−3 belong to this group. They increase and

(20) Chertihin, G. V.; Andrews, L. *J. Am. Chem. Soc.* **1994**, *116*, 8322.
(21) Lee, Y. K.; Manceron, L.; Papai, I. *J. Phys. Chem. A* **1997**, *101*, 9650.

Table 1. Frequencies of Observed Product Absorptions[a]

group	CH_3Cl	CD_3Cl	CH_3Br	CD_3Br
I	1618.4	1168.3	1619.0	1168.5
	773.9, **766.5**		774.7	
	643.8, **648.3**	517.2	648.4	**515.8**, 510.0
	631.0	504.1	628.6	503.4, **497.5**
II	1112.8	880.2	1112.7, 1108.9	875.3
	512.5	465.5	508.8	457.3
	412			
III	2887.4		2886.5	2092.6
	1373.4, 1372.3	1004.9	1370.4	1003.4
	1365.7		1367.9	
	1351.3			
		876.9		909.3
		869.4		903.1
		529.9, 527.9		
	566.5		527.7	432.2
	555.2	489.6	547.8	
	552.6	497.1	545.9	494.3
	423			

[a] All frequencies are in cm^{-1}. Stronger absorptions are in bold.

decrease repeatedly upon photolysis with UV (240 nm < λ < 380 nm) and visible (λ > 530 nm) light, respectively, and weaken gradually in the process of annealing.

Group II absorptions decrease by about 20% in intensity upon UV irradiation. They decay and grow repeatedly upon irradiation with UV and visible light, respectively, opposite to group I. They decrease rapidly upon annealing to higher than 20 K. No Ti−H stretching absorptions are included in this group. The opposite behaviors of groups I and II upon photolysis suggest that the two groups originate from different reaction products and that the reaction products are interconvertible in such a manner that an increase in concentration of one product leads to a decrease in concentration of the other product.

Group III absorptions are relatively weak in the original spectrum after co-deposition of methyl halide and laser-ablated Ti atoms. They grow gradually during photolysis, regardless of the wavelength, and once they grow, they do not decrease in the subsequent cycles of photolysis. In annealing, they grow dramatically up to 32 K. Figure 4 shows the variation in absorption intensity of the relatively strong group III absorptions of Ti + CH_3Cl upon annealing and at higher concentration: the intensities increase about 5 times in the process of annealing. Their relative intensities also increase considerably at high concentration of methyl halide in argon, as shown Figure 4.

Group I. The Ti−H stretching absorptions described above belong to group I. The observation of a metal−hydrogen stretching absorption indicates that C−H insertion by Ti occurs, and among the plausible products in the reaction of vaporized Ti atoms and methyl halides, the absorption most likely arises from the methylidene complex CH_2═TiHX.[9] The absorptions at 648.3 and 648.4 cm^{-1} in Figures 1 and 2 show isotopic shifts of −131.1 and −132.6 cm^{-1}, respectively, upon deuteration (H/D isotopic ratios of 1.253 and 1.257), and the strong absorptions at 631.0 and 628.6 cm^{-1} in Figures 1 and 2 show similar isotope shifts of −126.9 and −131.1 cm^{-1}, respectively, upon D substitution (H/D isotopic ratios of 1.252 and 1.264). The frequencies and isotope shifts show that the absorptions probably arise from hydrogen bending modes. The calculation results, given in Table 2, indicate that the absorptions probably arise from the CTiH in-plane bending and CH_2 wagging modes, respectively.

The Ti−Cl and Ti−Br stretching absorptions of CH_2═TiHX, unlike the case of methyl fluoride,[9−12] are not observed in this study, because of the low frequencies as shown in Table 2. On the other hand, new absorptions are observed at 766.5 and 774.7 cm^{-1} in Figures 1 and 2, respectively. The frequencies are 8.7 and 16.9 cm^{-1} higher than the corresponding one in the previous Ti + CH_3F study. Parallel to the previous studies, the absorptions are assigned to the predominately C═Ti stretching mode of the products. Cartesian coordinate displacements reveal large C and Ti movements but contribution from methylene hydrogen as well. In the CH_2═TiHF case, this mode at 757.8 cm^{-1} shifted to 748.8 cm^{-1} with $^{13}CH_3F$ and to 644.9 cm^{-1} with CD_3F, indicating mixing with a CH_2 motion. Because the CH_2 modes (ν_3 and ν_7, Table 2) are nearly the same for CH_2═TiHCl and CH_2═TiHBr, we expect comparable mode mixing, and we take the increase in the "predominately C═Ti" stretching mode to suggest that the C═Ti bonds of CH_2═TiHCl and CH_2═TiHBr are, in fact, stronger than that of CH_2═TiHF. This is consistent with the computed decrease in C═Ti bond lengths in the series. It is appropriate to note that the predominately C═Ti stretching mode observed for the CH_2═TiHX species (757.8, 766.5, and 774.7 cm^{-1}) are higher than the C═M stretching modes assigned for CH_2═M species (M = Cr−Zn, i.e., 567.0, 521.9, 623.9, 696.2,

Table 2. Observed and Calculated Fundamental Frequencies of CH_2═TiHCl and CH_2═TiHBr in the Ground Electronic State (^1A)[a]

	CH_2═TiHCl			CD_2═TiDCl			CH_2═TiHBr			CD_2═TiDBr		
description	exp	calc	int	exp	calc	int	exp	calc	int	exp	calc	int
ν_1 A′ C−H_2 stretch		3190.9	2		2362.9	4	3190.4	3			2362.6	5
ν_2 A′ C−H_1 stretch		2795.9	2		2034.2	2	2785.5	2			2066.6	2
ν_3 A′ Ti−H_3 stretch	1618.4	1680.2	400	1168.3	1201.8	211	1619.0	1680.6	402	1168.5	1202.0	211
ν_4 A′ CH_2 scissor		1340.6	24		1051.5	28		1343.2	23		1051.8	28
ν_5 A′ C−Ti stretch	766.5	822.7	88	727.4	57	774.7	823.8	85	729.4	55		
ν_6 A′ CTiH bend	648.3	693.2	45	517.2	548.4	58	648.4	693.7	29	515.8	539.2	62
ν_7 A′ CH_2 rock		442.4	11		330.5	4		452.9	10		335.9	5
ν_8 A′ Ti−X stretch		409.7	59		389.1	42		309.3	37		297.2	31
ν_9 A′ CTiX bend		147.4	4		133.5	3		131.0	4		118.6	3
ν_{10} A″ CH_2 wag	631.0	684.4	167	504.1	539.0	118	628.6	683.9	161	497.5	537.9	82
ν_{11} A″ CH_2 twist		487.9	28		345.7	12		479.3	30		339.3	14
ν_{12} A″ TiH OOP bend		65.0	138		49.7	82		65.5	122		49.1	72

[a] Frequencies and infrared intensities are in cm^{-1} and km/mol, respectively. Intensities are all calculated values.

Table 3. Observed and Calculated Fundamental Frequencies of CH_3TiCl and CH_3TiBr in the Ground Electronic States (^3A)[a]

	$CH_3-Ti-Cl$			$CD_3-Ti-Cl$			$CH_3-Ti-Br$			$CD_3-Ti-Br$		
description	exp	calc	int	exp	calc	int	exp	calc	int	exp	calc	int
ν_1 A′ CH_3 stretch		3084.0	4		2276.9	1		3084.0	4		2276.8	1
ν_2 A′ CH_3 stretch		2960.9	7		2124.7	1		2961.9	8		2125.4	1
ν_3 A′ CH_3 scissor		1414.2	1		1026.4	2		1412.8	2		1025.5	2
ν_4 A′ CH_3 deform.	1112.8	1146.0	8	880.2	901.8	22	1112.7	1146.1	7	875.3	901.8	21
ν_5 A′ C−Ti stretch	512.5	531.3	66	465.5	477.8	80	508.8	529.6	61	457.3	472.3	63
ν_6 A′ Ti−X stretch	412	432.3	120		405.1	81		399.5	77		332.5	72
ν_7 A′ CH_3 rock		362.8	4		298.2	5		287.7	23		267.0	3
ν_8 A′ CTiX bend		96.3	4		88.8	4		84.6	3		77.2	3
ν_9 A″ CH_3 stretch		3019.7	7		2230.1	2		3020.9	9		2230.9	3
ν_{10} A″ CH_3 scissor		1427.2	3		1035.3	3		1427.4	3		1035.4	3
ν_{11} A″ CH_3 rock		389.1	18		291.4	12		385.4 1	7		288.9 1	2
ν_{12} A″ CH_3 distort.		99.1	0		73.8	1		89.1	0		66.6	0

[a] Frequencies and intensities are in cm^{-1} and km/mol, respectively. Intensities are all calculated values.

Table 4. Observed and Calculated Fundamental Frequencies of $(CH_3)_2TiCl_2$[a]

	$(CH_3)_2TiCl_2$			$(CD_3)_2TiCl_2$		
description	exp	calc	int	exp	calc	int
ν_1 A_1 CH_3 stretch (a)		3094.0	3		2288.5	1
ν_2 A_1 CH_3 stretch (s)		3003.5	0		2148.9	1
ν_3 A_1 CH_3 scissor	1365.7	1413.9	9	*b*	1027.0	6
ν_4 A_1 CH_3 deform.		1160.2	4	876.9	914.8	12
ν_5 A_1 TiC_2 stretch (s)	552.6	561.2	83	497.1	509.9	78
ν_6 A_1 CH_3 rock		490.9	0		365.1	4
ν_7 A_1 $TiCl_2$ stretch (s)		396.2	27		404.5	15
ν_8 A_1 TiC_2 IP bend		155.9	0		136.6	0
ν_9 A_1 $TiCl_2$ bend		105.1	2		103.7	2
ν_{10} A_2 CH_3 stretch		3093.8	0		2289.9	0
ν_{11} A_2 CH_3 scissor		1408.6	0		1023.3	0
ν_{12} A_2 CH_3 rock		509.4	0		387.3	0
ν_{13} A_2 $TiCl_2$ twist		132.1	0		117.9	0
ν_{14} A_2 CH_3 distort.		88.1	0		62.8	0
ν_{15} B_1 CH_3 stretch		3097.1	8		2291.9	3
ν_{16} B_1 CH_3 scissor	1373.4	1415.3	17	1004.9	1027.3	10
ν_{17} B_1 CH_3 rock	566.5	579.2	94	529.9	526.8	142
ν_{18} B_1 $TiCl_2$ stretch (a)	423	438.5	67		366.5	16
ν_{19} B_1 $TiCl_2$ rock		151.5	0		137.3	0
ν_{20} B_1 CH_3 distort.		114.5	0		81.4	0
ν_{21} B_2 CH_3 stretch (a)		3094.3	1		2289.8	0
ν_{22} B_2 CH_3 stretch (s)	2887.4	3001.6	1		2147.4	2
ν_{23} B_2 CH_3 scissor	1351.3	1405.6	7		1020.9	4
ν_{24} B_2 CH_3 deform.		1147.8	4	869.4	912.4	19
ν_{25} B_2 TiC_2 stretch (a)	555.2	560.6	82	489.6	504.6	67
ν_{26} B_2 CH_3 rock		473.0	3		357.9	0
ν_{27} B_2 $TiCl_2$ OOP bend		128.9	3		122.3	2

[a] Frequencies and intensities are in cm^{-1} and km/mol, respectively. Calculations were done at the B3LYP/6-311++G(2d,p) level.

Table 5. Observed and Calculated Fundamental Frequencies of $(CH_3)_2TiBr_2$[a]

	$(CH_3)_2TiBr_2$			$(CD_3)_2TiBr_2$		
description	exp	calc	int	exp	calc	int
ν_1 A_1 CH_3 stretch (a)		3094.6	2		2288.9	0
ν_2 A_1 CH_3 stretch (s)		3003.0	0		2148.4	1
ν_3 A_1 CH_3 scissor	1367.9	1412.7	10	*b*	1026.2	6
ν_4 A_1 CH_3 deform.		1157.1	3	909.3	912.8	12
ν_5 A_1 TiC_2 stretch (s)	545.9	555.1	72	494.3	501.1	60
ν_6 A_1 CH_3 rock		484.3	0		377.5	2
ν_7 A_1 $TiBr_2$ stretch (s)		282.6	17		274.2	13
ν_8 A_1 TiC_2 IP bend		150.5	0		131.9	0
ν_9 A_1 $TiBr_2$ bend		72.7	0		71.9	0
ν_{10} A_2 CH_3 stretch		3092.8	0		2288.9	0
ν_{11} A_2 CH_3 scissor		1406.8	0		1022.2	0
ν_{12} A_2 CH_3 rock		497.7	0		377.1	0
ν_{13} A_2 $TiBr_2$ twist		123.8	0		108.5	0
ν_{14} A_2 CH_3 distort.		94.0	0		67.0	0
ν_{15} B_1 CH_3 stretch		3096.1	8	2232	2291.1	3
ν_{16} B_1 CH_3 scissor	1370.4	1413.5	19	1003.4	1026.2	11
ν_{17} B_1 CH_3 rock	527.7	543.5	37	432.2	459.8	73
ν_{18} B_1 $TiBr_2$ stretch (a)		364.7	71		324.1	35
ν_{19} B_1 $TiBr_2$ rock		134.0	2		120.8	1
ν_{20} B_1 CH_3 distort.		121.6	0		86.3	0
ν_{21} B_2 CH_3 stretch (a)		3094.8	0		2290.2	0
ν_{22} B_2 CH_3 stretch (s)	2886.5	3001.1	2	2092.6	2146.9	3
ν_{23} B_2 CH_3 scissor	1360.0	1404.0	6		1019.8	3
ν_{24} B_2 CH_3 deform.		1145.0	5	903.1	910.7	20
ν_{25} B_2 TiC_2 stretch (a)	547.8	556.4	73	494.3	500.6	58
ν_{26} B_2 CH_3 rock		468.7	3		354.0	0
ν_{27} B_2 $TiBr_2$ OOP bend		113.3	1		106.7	1

[a] Frequencies and intensities are in cm^{-1} and km/mol, respectively. Calculations were done at the B3LYP/6-311++G(2d,p) level. [b] Overlapped.

614.0, and 513.7 cm^{-1}, respectively),[8] but the latter modes are higher in C═M character according to the observed ^{13}C═M shifts.

As with formation of simple methylidene complexes in reactions of CH_3F with vaporized group IV transition metals,[9,11−14] the present results show that methylidene complexes can also be generated from other methyl halides with vaporized transition-metal atoms or UV photolysis. Moreover, CH_3Cl and CH_3Br are clearly more reactive than CH_3F.

Group II. Figures 1−3 show that the compound responsible for group II is formed originally in a relatively large amount in reaction of methyl halide and Ti atoms, in comparison with the methylidene complex. The strongest absorptions of group II are observed at 512.5 and 508.8 cm^{-1} in the spectra of Ti + CH_3Cl and Ti + CH_3Br as shown in Figures 1 and 2, and they exhibit relatively small isotopic shifts of −46.5 and −51.5 cm^{-1}, respectively (H/D isotopic ratios of 1.101 and 1.113), upon deuteration. The absorptions are assigned to the C−Ti stretching mode. The absorptions at 1112.8 and 1112.7 cm^{-1} show isotopic shifts of −232.6 and −237.4 cm^{-1}, respectively, upon D substitution (H/D isotopic ratios of 1.264 and 1.271), and on the basis of the frequencies and the isotopic shifts, they are attributed to a hydrogen deformation mode of the products. The absorption at 412 cm^{-1} in the spectrum of Ti + CH_3Cl is assigned to the Ti−Cl stretching mode of the product, which is close to the Ti−Cl stretching frequency of the TiCl radical (404.33 cm^{-1}) in the ground electronic state ($X^4\Phi$).[22]

(22) Imajo, T.; Wang, D.; Tanaka, K.; Tanaka, T. *J. Mol. Spectrosc.* **2000**, *203*, 216.

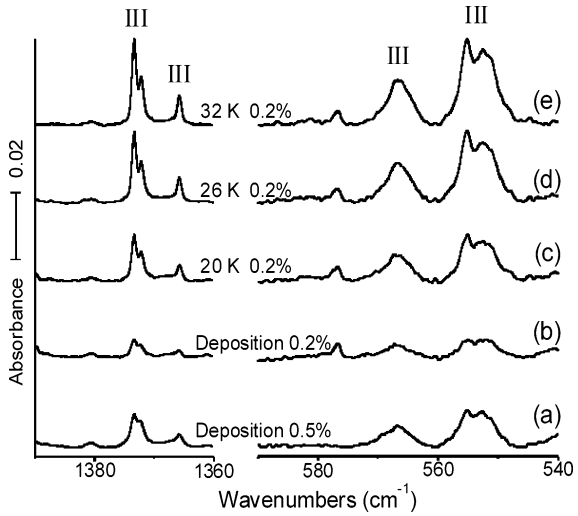

Figure 4. IR spectra in the regions of 1360−1400 and 540−600 cm^{-1} for laser-ablated Ti atoms co-deposited with CH_3Cl diluted in Ar at 7 K. (a) Ti + 0.5% CH_3Cl in Ar co-deposited for 1 h. (b) Ti + 0.2% CH_3Cl in Ar co-deposited for 1 h. (c−e) After annealing to 20, 26, and 32 K, respectively, following co-deposition of Ti + 0.2% CH_3F in Ar for 1 h.

It should be remembered at this point that the most stable compound among the plausible products in the reaction of methyl halide with vaporized Ti atoms is CH_3-TiX in its triplet ground state.[9] Calculations show that the approach of a Ti atom ($^3F_2$) to methyl halide on the side of halogen atom eventually leads to the structure of CH_3TiX (T) on the triplet potential energy surface. Table 3 shows that the group II absorptions in Figures 1 and 2 match with the predicted strong absorptions of CH_3TiCl and CH_3TiBr. The present results indicate that, parallel to the case of Ti + CH_3F, CH_3-TiCl and CH_3TiBr are produced mostly in the reaction of vaporized Ti atoms with methyl chloride and bromide.

Therefore, CH_3MX is evidently first formed in reaction of methyl halide with laser-ablated transition-metal atoms and then transformed to the methylidene complex or larger complexes, even during co-deposition. Formation of CH_3-MX requires activation energy, laser ablation provides excited transition-metal atoms,[17] and the excited intermediate thus formed can be relaxed by the matrix or undergo α-hydrogen transfer.[23]

$$CH_3X + M^* \rightarrow [CH_3MX]^* \rightarrow CH_2{=}MHX \qquad (1)$$

Apparently, the conversion of the Grignard-type product to the methylidene complex takes place most efficiently in a system where the energy of the methylidene complex is comparable to that of the Grignard-type complex.

In the titanium systems, the Grignard-type products are most stable, relative to the corresponding methylidene complex, among the Grignard-type complexes derived from group IV transition metals (CH_3TiX, CH_3ZrX, and CH_3HfX). The energy differences are more than 20 kcal/mol at the current level of theory (Tables 6 and 7 here and Table 6 in ref 9). Studies show that CH_3TiX is mostly produced in the reaction of vaporized Ti atoms and methyl halide, and CH_2=TiHX is formed initially only in a relatively small amount.[9,10] The methylidene complex is increased several fold upon subsequent UV photolysis to promote α-H transfer.

Table 6. Calculated Geometrical Parameters and Physical Constants of CH_2=TiHCl, CH_3−TiCl, and $(CH_3)_2TiCl_2$[a]

parameter	CH_2=TiHCl	CH_3−TiCl	$(CH_3)_2TiCl_2$
r(C−H_1)	1.123	1.093	1.094
r(C−H_2)	1.085	1.100	1.094
r(C−Ti)	1.801	2.107	2.053
r(Ti−H_3)	1.733		
r(Ti−Cl)	2.244	2.260	2.213
r(Ti···H_1)	2.070	2.753	2.622
∠H_1CH_2	114.4	108.1	109.6
∠H_2CH_3		107.6	110.1
∠CTiCl	122.6	130.0	108.3
∠$CTiH_3$	111.1		
∠H_3TiCl	126.3		
∠H_1CTi	86.9	115.0	109.0
∠H_2CTi	158.7	108.9	109.2
Φ(H_1CTiH_3)	0.0	121.4	119.8
Φ(H_1CTiCl)	180.0	0.0	64.7
mol symm	C_s	C_s	C_{2v}
q(C)[b]	−0.44	−0.59	−0.39
q(H_1)[b]	0.13	0.12	0.15
q(H_2)[b]	0.15	0.10	0.15
q(H_3)[b]	−0.18	0.10	0.15
q(Ti)[b]	0.60	0.62	0.17
q(Cl)[b]	−0.26	−0.35	−0.14
μ[c]	1.43	3.27	2.04
state[d]	$^1A'$	$^3A''$	$^1A_1$
ΔE[e,f]	102.2[g]	124.2[h]	203.0

[a] Bond lengths and angles are in angstroms and degrees, respectively. [b] Mulliken atomic charge. [c] Molecular dipole moments are in debye. [d] Electronic state. [e] Binding energies in kcal/mol. [f] Transition state binding energies: T, 86.0 kcal/mol, and S, 87.1 kcal/mol. [g] Lowest triplet state binding energy is 90.0 kcal/mol. [h] Lowest singlet state binding energy is 99.1 kcal/mol.

Table 7. Calculated Geometrical Parameters and Physical Constants of CH_2=TiHBr, CH_3−TiBr, and $(CH_3)_2TiBr_2$[a]

parameter	CH_2=TiHBr	CH_3−TiBr	$(CH_3)_2TiBr_2$
r(C−H_1)	1.125	1.093	1.094
r(C−H_2)	1.085	1.100	1.094
r(C−Ti)	1.798	2.107	2.052
r(Ti−H_3)	1.731		
r(Ti−Br)	2.403	2.421	2.372
r(Ti···H_1)	2.055	2.759	2.621
∠H_1CH_2	114.4	108.0	109.7
∠H_2CH_3		107.7	110.1
∠CTiBr	122.8	131.3	108.5
∠$CTiH_3$	110.6		
∠H_3TiBr	126.6		
∠H_1CTi	86.1	115.4	109.0
∠H_2CTi	159.5	108.8	109.2
Φ(H_1CTiH_3)		121.5	119.8
Φ(H_1CTiBr)		0.0	64.7
mol symm	C_s	C_s	C_{2v}
q(C)[b]	−0.44	−0.63	−0.60
q(H_1)[b]	0.14	0.13	0.12
q(H_2)[b]	0.16	0.10	0.14
q(H_3)[b]	−0.17	0.10	0.14
q(Ti)[b]	0.67	0.77	1.37
q(Br)[b]	−0.37	−0.47	−0.48
μ[c]	1.48	3.35	1.99
state[d]	$^1A'$	$^3A''$	$^1A_1$
ΔE[e,f]	100.4[g]	123.1[h]	198.4

[a] Bond lengths and angles are in angstroms and degrees, respectively. [b] Mulliken atomic charge. [c] Molecular dipole moments are in debye. [d] Electronic state. [e] Binding energies in kcal/mol. [f] Transition state binding energies: T, 84.6 kcal/mol and S, 86.4 kcal/mol. [g] Lowest triplet state binding energy is 90.2 kcal/mol. [h] Lowest singlet state binding energy is 97.3 kcal/mol.

(23) Crabtree, R. H. *The Organometallic Chemistry of the Transition Metals*; Wiley and Sons: New York, 2001; p 190.

On the other hand, in the zirconium systems, the energy difference between CH_3ZrX and $CH_2{=}ZrHX$ is 10−20 kcal/mol, and both the Grignard-type and methylidene complexes are produced in reaction of methyl fluoride with vaporized Zr atoms.[11] In the Hf system, the Grignard-type and methylidene complexes are comparable in energy, and CH_3-HfF is not identified in the spectrum of Hf + CH_3F, but strong absorptions from the methylidene complex are observed.[12]

For justification of the relative yield of the methylidene complex, the further stabilization of the reaction products in the matrix should also be considered. The interaction between the metal atom and Ar matrix is expected to be stronger for the methylidene complex, because of the higher electron deficiency caused by the higher oxidation state of the metal atom.[1] Calculations show that an Ar atom can be easily coordinated to the metal atom of the methylidene complex, about 2.74 Å apart above or below the molecular plane. The binding energy of a single Ar atom is about 2 kcal/mol. Therefore, in the case of the Hf system, the actual energy of the methylidene complex could well be lower than that of the Grignard-type product.

Group III. The group III absorptions in Figures 1−3 increase dramatically upon annealing. The variation is shown in Figure 4; the group III absorptions in the regions of 540−600 and 1360−1400 cm^{-1} for Ti + CH_3Cl increase substantially at high concentration of CH_3Cl as well as on annealing. This indicates that group III absorptions arise from a larger complex. It was previously reported that $(CH_3)_2TiF_2$ is produced in the reaction of vaporized Ti atoms with CH_3F, whose absorptions grow significantly upon annealing and at high CH_3F concentration.[10] The product absorptions including Ti−C_2 antisymmetric stretching and Ti−F_2 symmetric and antisymmetric stretching absorptions, along with the satellite absorptions caused by the Ti isotopes, are observed, and the calculation results with the C_{2v} structure show excellent agreement with the observed values.

Martinsky and Minot theoretically studied the structures of titanium chloride complexes including dinuclear and dihalide complexes.[24] Kaupp predicted the C_{2v} structure of dimethyl titanium dichloride and argued on the basis of NBO/NLMO analyses that the influence of ligand-to-metal π-bond should be very significant on the bond angles.[25] More recently, however, it was shown by computation that the bond angles of $(CH_3)_2TiF_2$ are very close to those of $(CH_3)_2TiCl_2$.[10] McGrady et al. prepared $(CH_3)_2TiCl_2$ in the reaction $Me_2Zn + TiCl_4 \rightarrow Me_2TiCl_2 + ZnCl_2$ under high vacuum and rigorously moistureless conditions and observed the spectra in the gas phase and inert matrixes (Ar and N_2).[26]

The vibrational characteristics of group III absorptions of Ti + CH_3Cl are basically consistent with the previous results for $(CH_3)_2TiCl_2$ obtained by McGrady et al.[26] Most Ar matrix frequencies (measured at an optimum resolution of 1.7 cm^{-1}) in the previous study match within 3 cm^{-1} with the group III frequencies. The group III frequencies are also compared with the calculated values in Table 4, showing good agreement, and they turned out to be the relatively strong absorptions observed in the previous study and also predicted in calculations. The present results, along with previous ones, indicate that $(CH_3)_2TiCl_2$ is indeed produced in the reaction of CH_3Cl with vaporized Ti atoms and isolated in a solid Ar matrix.

The vibrational characteristics of group III absorptions in the Ti + CH_3Br spectra and their variation upon annealing and concentration change follow those of Ti + CH_3Cl, and the observed frequencies are compared with the values calculated for $(CH_3)_2TiBr_2$ with a C_{2v} structure in Table 5, showing good agreement. This indicates that $(CH_3)_2TiBr_2$ is formed for the first time, and reaction of vaporized Ti atoms with alkyl halide is a very efficient method to synthesize dialkyl titanium dihalide compounds.

The general formation of $(CH_3)_2TiX_2$ in the reaction of vaporized Ti atoms and methyl halides and the remarkable increase of the concentration most probably result from the fact that $(CH_3)_2TiX_2$ is much more stable than CH_3TiX and $CH_2{=}TiHX$. The binding energies of $(CH_3)_2TiCl_2$ and $(CH_3)_2TiBr_2$ are compared with those of smaller reaction products (CH_3TiX and $CH_2{=}TiHX$) in Tables 6 and 7. The stability of dimethyl titanium dichloride has also been demonstrated experimentally.[26] Our experiments show that, once formed in the matrix, $(CH_3)_2TiX_2$ does not decompose in the process of photolysis and annealing until the Ar matrix evaporates.

It is not clear at this point whether $(CH_3)_2TiX_2$ is formed from CH_3TiX or $CH_2{=}TiHX$. The CH_3TiX molecule has a triplet ground state, which is expected to be reactive with CH_3X located nearby in the matrix. Insertion into the C−X bond of CH_3X by CH_3TiX should readily occur to form $(CH_3)_2TiX_2$, similar to the C−X insertion of CH_3X by the triplet Ti atom ($^3F_2$) to produce CH_3TiX.

$$CH_3TiCl\ (T) + CH_3Cl\ (S) \rightarrow (CH_3)_2TiCl_2\ (S) \qquad \Delta E = -79\ \text{kcal/mol} \quad (2)$$

$$CH_3TiBr\ (T) + CH_3Br\ (S) \rightarrow (CH_3)_2TiBr_2\ (S) \qquad \Delta E = -75\ \text{kcal/mol} \quad (3)$$

On the other hand, alkylidene complexes are well-known C−H activation agents,[1−4,15,16] and therefore, C−H activation of CH_3X by $CH_2{=}TiHX$ and subsequent rearrangement might result in formation of $(CH_3)_2TiX_2$. The C−H activation by an alkylidene complex appears similar to a typical addition reaction to a double bond.

$$CH_2{=}TiHCl + H{-}CH_2Cl \rightarrow CH_3{-}TiHCl{-}CH_2Cl \rightarrow (CH_3)_2TiCl_2 \qquad \Delta E = -101\ \text{kcal/mol} \quad (4)$$

$$CH_2{=}TiHBr + H{-}CH_2Br \rightarrow CH_3{-}TiHBr{-}CH_2Br \rightarrow (CH_3)_2TiBr_2 \qquad \Delta E = -98\ \text{kcal/mol} \quad (5)$$

It is also possible that both CH_3TiX and $CH_2{=}TiHX$ react with CH_3X nearby in the matrix to form $(CH_3)_2TiX_2$. Further

(24) Martinsky, C.; Minot, C. *Surface Sci*. **2000**, *467*, 152.
(25) Kaupp, M. *Chem. Eur. J*. **1999**, *5*, 3631.
(26) (a) McGrady, G. S.; Downs, A. J.; Bednall, N. C.; McKean, D. C.; Thiel, W.; Jonas, V.; Frenking, G.; Scherer, W. *J. Phys. Chem. A* **1997**, *101*, 1951. (b) McGrady, G. S.; Downs, A. J.; McKean, D. C.; Haaland, A.; Scherer, W.; Verne, H. P.; Volden, H. V. *Inorg. Chem.* **1996**, *35*, 4713.

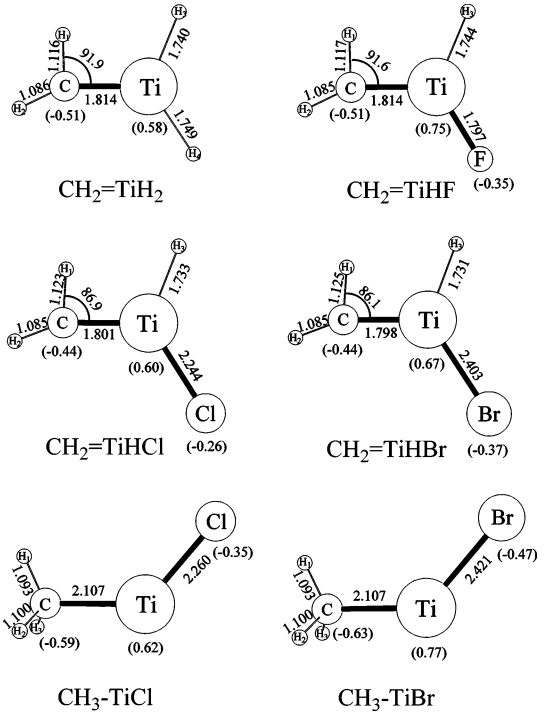

Figure 5. Optimized molecular structures for Ti−methylidene and Grignard-type complexes. The bond lengths and angles are in Å and degrees, respectively, and the numbers in parentheses are the Mulliken charges of the carbon, titanium, and halogen atoms. The methylene group is noticeably distorted, and one of the methylene hydrogen atoms is very close to the Ti atom, indicating that there is strong agostic interaction between the atoms. All-electron calculations carried out using B3LYP and the 6-311++G(2d,p) basis set.

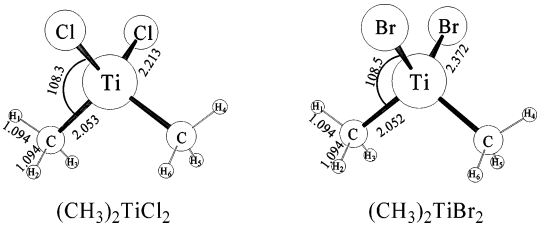

Figure 6. Optimized structures of the $(CH_3)_2TiCl_2$ and $(CH_3)_2TiBr_2$ complexes. The bond lengths and angles are in angstroms and degrees, respectively. All-electron calculations carried out using B3LYP and the 6-311++G(2d,p) basis set.

study will be necessary to determine the mechanism of formation of the dialkyl titanium dihalide complex.

Several other absorptions are common to different metal experiments. Weak absorptions at 825.9, 820.1 cm^{-1} and 788.1, 781.5 cm^{-1} are due to the CH_2Cl and CD_2Cl free radicals with resolved ^{35}Cl, ^{37}Cl isotopic absorptions, and similar weak 692.8 and 655.0 cm^{-1} bands are due to the CH_2Br and CD_2Br free radicals.[27,28] Recall that the CH_2F and CD_2F free radicals were observed in similar methyl fluoride experiments.[9] Radiation from the laser ablation plume is capable of precursor photodissociation.

Molecular Structures. The optimized geometries of the major products from reaction of CH_3Cl and CH_3Br with laser-ablated Ti atoms are shown in Figures 5 and 6, and the geometrical parameters are summarized in Tables 6 and 7. The methylidene and Grignard-type complexes have (C_s) structures. It is worth mentioning that both MP2 and DFT methods with LanL or SDD effective core potential and basis set for Ti lead to C_1 structures for the methylidene complex with Ti and C atoms serving as trigonal pyramidal apexes, as found for $CH_2{=}ZrH_2$.[13,14] On the other hand, the all-electron basis for Ti yields a planar methylidene.

The C−Ti bond length of the methylidene complex is much shorter than that of the Grignard-type complex, reflecting the higher bond order. The $(CH_3)_2TiCl_2$ and $(CH_3)_2TiBr_2$ molecules (Figure 6) and the previously[10] studied $(CH_3)_2TiF_2$ all have almost identical C_{2v} structures and geometrical parameters including the X−Ti−X angle (∠XTiX), other than the Ti−X bond lengths. The geometrical parameters of $(CH_3)_2TiCl_2$ in Table 6 are consistent with theoretical and experimental results.[25,26] This suggests that the ligand-to-metal π bond does not affect the bond angles substantially.

In the structures of the methylidene complexes shown in Figure 5, the distorted CH_2 group due to strong agostic interaction between the metal atom and one of the α-hydrogen atoms is evident, along with the elongated C−H bond. ∠H_1CTi is less than 90.0°, and the distance between one of the methylene hydrogen atoms and the Ti atom is only 2.070 and 2.055 Å for $CH_2{=}$TiHCl and $CH_2{=}$TiHBr, respectively. Agostic interactions have been found to be quite common, provided a metal has a low-lying empty valence orbital and a C−H bond in reasonable proximity.[15−17] It is implicit that this interaction involves attraction between the electron-deficient metal center and the C−H bond acting as a Lewis base, which forms at the expense of a significant distortion within the ligand including bending at CH_2 and lengthening of the C−H bond in order to stabilize the C=Ti bond.

For comparison, the same all-electron basis calculation has been performed for $CH_2{=}TiH_2$ and $CH_2{=}$TiHF, and the structures are also shown in Figure 5. Early calculations of $CH_2{=}TiH_2$ failed to find the agostic interaction[5,6] owing to the lack of polarization functions in the basis set. More recent work has noted the importance of polarization functions to characterize the agostic interaction.[16]

In a methylidene complex, the simplest alkylidene complex, the strength of the agostic interaction can be roughly estimated by the H_1−C−M angle (∠H_1CM), the C=Ti bond length, and the distance between the interacting α-hydrogen and metal atoms. Among the titanium methylidene complexes, the agostic interaction increases in the order of $CH_2{=}TiH_2$, $CH_2{=}$TiHF, $CH_2{=}$TiHCl, and $CH_2{=}$TiHBr as determined by calculated values using all-electron basis sets (∠H_1CTi = 91.9, 91.6, 86.9, and 86.1°); C=Ti bond lengths $CH_2{=}TiH_2$ (1.814 Å), $CH_2{=}$TiHF (1.814 Å), $CH_2{=}$TiHCl (1.801 Å), and $CH_2{=}$TiHBr (1.798 Å); and $r(Ti\cdots H_1)$ = 2.161, 2.156, 2.070, and 2.055 Å, respectively. The variation is also consistent with the observed predominately C=Ti stretching frequencies of $CH_2{=}$TiHF (757.8 cm^{-1}), $CH_2{=}$TiHCl (766.5 cm^{-1}), and $CH_2{=}$TiHBr (774.7 cm^{-1}).

The Photoreversible System. Parallel to the case of Ti + CH_3F,[9] the methylidene and Grignard-type complexes

(27) Andrews, L.; Smith, D. W. *J. Chem. Phys.* **1970**, *53*, 2956.
(28) Smith, D. W.; Andrews, L. *J. Chem. Phys.* **1971**, *55*, 5295.

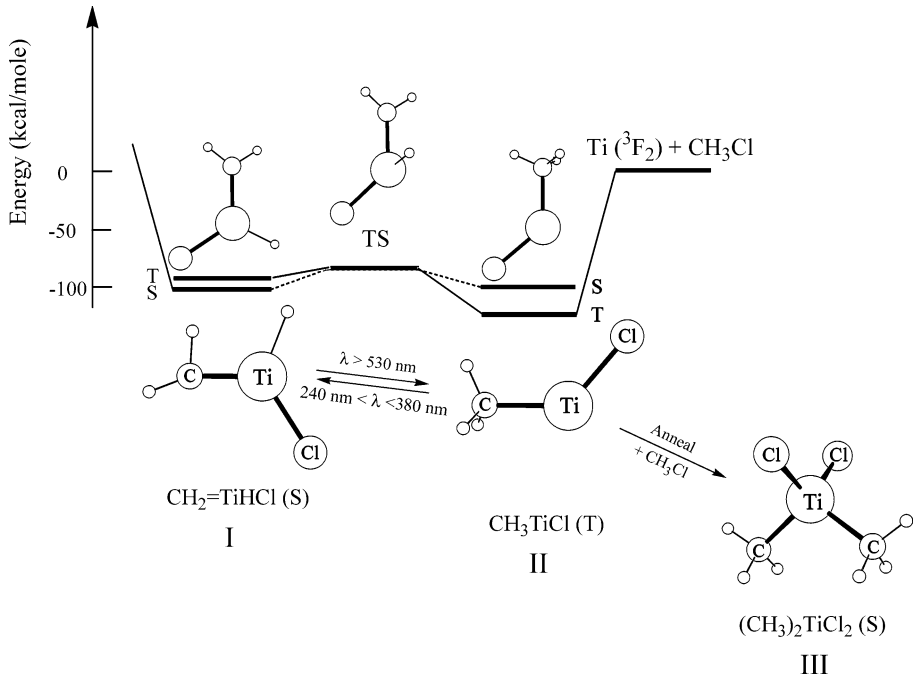

Figure 7. The photoreversible system identified in this study. CH_3TiCl is converted to CH_2═TiHCl by UV (240 nm < λ < 380 nm) irradiation and vice versa by visible (λ > 530 nm) irradiation. Intersystem crossings inevitably accompany the conversions (see text). Structures and energies are from all-electron B3LYP calculations. The transition state (TS) is the optimized triplet with C_1 symmetry; the singlet TS has a slightly different structure and nearly the same energy.

form persistent photoreversible systems between CH_3TiX and CH_2═TiHX via α-hydrogen migration. The photoreversible Ti + CH_3Cl system is illustrated in Figure 7, and that for Ti + CH_3Br is essentially the same. In the reaction of methyl halide and laser-ablated Ti atoms, CH_3TiX is initially generated mostly, perhaps because of the relative stability of the Grignard-type product. UV photolysis (240 nm < λ < 380 nm) transforms CH_3TiX to CH_2═TiHX, whereas photolysis with visible light (λ > 530 nm) reverses the effect.

As listed in Tables 6 and 7, the methylidene and Grignard-type complexes have singlet and triplet ground states, respectively.[9] Therefore, interconversions between the complexes must involve intersystem crossings. The lowest triplet and singlet states of CH_2═TiHCl and CH_3TiCl are computed to be 10.2 and 25.1 kcal/mol above the singlet and triplet ground states, respectively, and those of CH_2═TiHBr and CH_3TiBr are 10.2 and 25.8 kcal/mol above the corresponding ground states, respectively. Starting with triplet ground state CH_3TiCl, UV excitation to the triplet transition state 38.2 kcal/mol higher leads to the triplet CH_2═TiHCl, which intersystem crosses to the more stable singlet CH_2═TiHCl ground state. In the reverse process, visible excitation of singlet CH_2═TiHCl to the singlet transition state 15.1 kcal/mol higher gives singlet CH_3TiCl, which intersystem crosses to the triplet CH_3TiCl ground state. The photochemistry of triplet CH_3TiBr and singlet CH_2═TiHBr proceeds in like fashion.

Although the methylidene complex also has a planar structure in the lowest triplet state, our calculations show that the CH_2 group is not distorted in contrast to the ground singlet state. Apparently, the agostic interaction/distortion is observed only in the ground singlet state with the shorter C═Ti bond, which is consistent with the previous studies of methylidene complexes produced from transition-metal vapor and methyl halide or methane.[9,11,12,14] On the other hand, CH_3TiX has a C_s structure similar to that in the ground triplet state, where the halide, titanium, and carbon atoms and one of the hydrogen atoms are in the same plane.

This persistent photoreversible system terminates by further reaction of the products with methyl halide available in the matrix to a larger complex upon annealing. This and previous studies show that only a small amount of $(CH_3)_2TiX_2$ is formed initially in reaction of methyl halide and vaporized Ti; however, upon annealing, further reaction with available methyl halide increases the concentration dramatically.[9] The $(CH_3)_2TiX_2$ molecules are quite stable. Once the complex is formed, it does not dissociate back to the smaller precursors upon repeated photolysis and further annealing.

Conclusions

Reactions of laser-ablated Ti atoms with methyl halides (CH_3Cl and CH_3Br) in excess argon have been carried out during condensation at 7 K, and we find that CH_3Cl and CH_3Br are more reactive with the metal atoms than CH_4 and CH_3F. On the basis of the behaviors occurring upon photolysis and annealing, the product absorptions are sorted into three groups. Group I is relatively weak after co-deposition of methyl halide and the metal atoms but grows significantly upon UV irradiation and then repeatedly decreases and increases following visible (λ > 530 nm) and UV (240 nm < λ < 380 nm) irradiations, and group II shows the reverse trend. Spectroscopic evidence and DFT calculations, along with previous results, indicate that groups I and II arise from CH_2═TiHX and CH_3−TiX, and they define a persistent photoreversible system via α-hydrogen migration.

The molecular structures of CH_2═TiHCl and CH_2═TiHBr show evidence of agostic interaction between the metal atom and one of the α-hydrogen atoms in the ground singlet state. The strength of this agostic interaction increases in the order of CH_2═TiH_2, CH_2═TiHF, CH_2═TiHCl, and CH_2═TiHBr on the basis of the magnitude of CH_2 distortion, the distance between the α-hydrogen and titanium atoms, and the C═Ti bond stabilization. Ongoing investigation in this laboratory finds an even stronger agostic interaction in the corresponding iodide CH_2═TiHI. Group III grows only slightly in the cycles of photolysis but increases dramatically upon annealing, whereas groups I and II decrease substantially. Group III is identified as $(CH_3)_2TiX_2$, which is substantially more stable than the smaller complexes. The dimethyl titanium dihalides $(CH_3)_2TiF_2$, $(CH_3)_2TiCl_2$, and $(CH_3)_2TiBr_2$ all have very similar C_{2v} structures.

Acknowledgment. We gratefully acknowledge financial support for this work from NSF Grant CHE 03-52487 and sabbatical leave support (H.-G.C.) from the Korea Research Foundation (KRF-2003-013-C00044).

IC048615A